Proceedings of International Conference on Heat Exchanger Fouling and Cleaning - 2015 (Peer-reviewed)
June 07 - 12, 2015, Enfield (Dublin), Ireland
Editors: M.R. Malayeri, H. Müller-Steinhagen and A.P. Watkinson

Published online
www.heatexchanger-fouling.com

THE ROLE OF THERMOPHORESIS DURING DEPOSIT BUILD-UP ON A SUPERHEATER TUBE

U.S. Kleinhans[1*], M. Barnerßoi[1], S. Babat[2], C. Wieland[1] and H. Spliethoff[1,3]

[1] Institute for Energy Systems, Technische Universität München, Boltzmannstr. 15, 85748 Garching, Germany
[2] Institute of Combustion and Power Plant Technology, Pfaffenwaldring 23, 70569 Stuttgart, Germany
[3] ZAE Bayern (Center for Applied Energy Research), Walther-Meissner-Str. 6, 85748 Garching, Germany
*Email: ulrich.kleinhans@tum.de

ABSTRACT

Most studies on modelling ash deposition in pulverised fuel boilers focus on inertial impaction as the main deposition mechanism. Effects, such as thermophoresis or heterogeneous condensation, are often neglected. However, there are several studies indicating that thermophoresis plays a key role during the early stages of deposit build-up on a superheater tube.
Presented results obtained by numerical simulation show the dominant role of thermophoresis for small particle diameters, below 20 µm. It is shown that the capture efficiency increases by more than three orders of magnitude for particles in this size range and a temperature gradient of 380 K/mm in the boundary layer of the superheater tube. Furthermore, it is predicted that small iron-rich particles show a lowered deposition probability due to the increased thermal conductivity, compared to aluminosilicate particles. This behaviour was confirmed by measurements in a power plant.

INTRODUCTION

Ash deposition is one of the main reasons for unscheduled outages of coal-fired power plants. A lot of effort has been devoted in order to understand mechanisms and processes occurring inside a boiler. Baxter 1993 summarised four main ash deposition mechanisms as inertial impaction, thermophoresis, condensation effects, and chemical reactions. Inertial impaction is often considered as the main mechanism leading to extensive deposit build-up. All three other mechanisms are temperature-driven and often not addressed in modelling studies.

Thermophoresis (TP) is a force on small particles in a flow with a non-uniform temperature field. The thermophoretic force acts in the opposite direction to the temperature gradient, leading to an acceleration towards colder heat-exchanging surfaces. Responsible for this force is the increased kinetic energy of molecules at the hot particle surface, compared to the colder side of a particle. However, it is still not completely understood and often the subject of current research. Studies by Walker et al. 1979 or Cameron et al. 1999 showed that thermophoresis is the dominant deposition mechanism for particles in the diameter range of 0.1 to 10 µm. However, experiments are difficult to conduct, since thermophoretic forces for small particles are in the range of 10^{-9} to 10^{-15} N. It is, therefore, not surprising that experimental results measuring this small force show a broad scattering (see also Young 2011).

Many CFD studies on modelling ash deposition in furnaces use simplified methods correlating particle concentration in the near wall region to measured deposition rates from small scale experiments (see Kaer et al. 2006 for example). The main reason is due to the significantly higher number of cells required in order to resolve the boundary layers of heat-exchanging surfaces in a boiler. Numerical studies using resolved boundary layers are rare (see Haugen and Kragset 2010, Weber 2012 for example). The present paper, therefore, investigates the role of thermophoresis on deposition rates on a superheater tube, with a highly resolved boundary layer. A detailed particle transport model and different models for the thermophoretic force are investigated. Numerical simulation is based on power plant measurements described in the following section.

POWER PLANT MEASUREMENTS

Measurements conducted in a 302 MW_{el} combined heat and power plant located in Altbach, Germany, are used as boundary conditions for the numerical model. Fig. 1 shows a

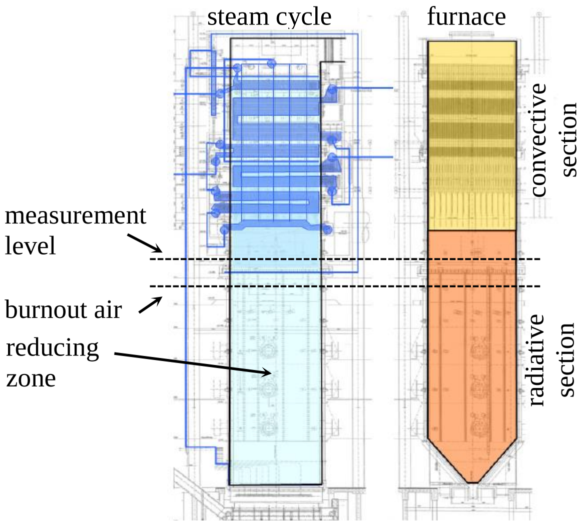

Fig. 1 Schematic of the 302 MW_{el} power plant indicating the position of measurements (see also Babat et al. 2014 or Sauer 2005).

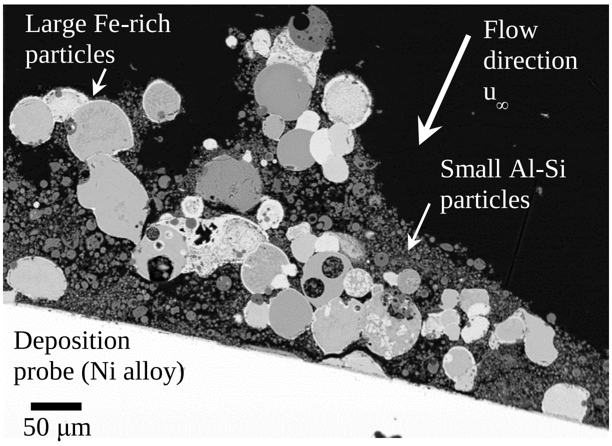

Fig. 2 SEM picture of a cooled deposit taken in the radiant superheater region (from Babat et al. 2014).

schematic of the pulverised fuel (PF) boiler. A cooled deposition probe was used, in combination with flue gas measurements and fly ash sampling. Experimental results are summarised by Babat et al. 2014. The deposition probe was inserted in the furnace just before the first superheater and, in subsequent steps, embedded in epoxy resin, cut and polished. The prepared coupons were investigated by a scanning electron microscope (SEM) and energy-dispersive X-ray (EDX) analysis. The emphasis was on particle sizes and their chemical composition. Fig. 2 shows a back-scattered electron image of the initial layer formed on the tube windward side after 231 hours of exposure. The deposit is composed of large iron-rich particles (diameter > 20 μm) and smaller particles mainly composed of aluminosilicates. Babat et al. 2014 explains the deposition of large iron-rich particles by the formation of a low-melting eutectic in the reducing burner region. These high density particles, with a high molten fraction, are transported to the surface by inertial impaction. Smaller particles (diameter < 20 μm) just above the initial layer are assumed to impact due to thermophoresis.

Flow characteristics at the location of the deposition probe in the Altbach PF boiler are summarised in Table 1. Values given in the right column of Table 1 are mean values of the measurements. The cooled deposition probe was controlled to a relatively high temperature of 690 °C and composed of the Nickel alloy 740 for the use in future power plants with increased steam temperatures. Fly ash was sampled and analysed by laser diffraction to determine particle size distribution (PSD). The d_{50} particle diameter of the fly ash was 21.4 μm. In addition, expected minima and maxima in typical PF systems are given in Table 1 and used to estimate the flow and heat transfer characteristics around a superheater tube in a cross-flow. Expected dimensionless numbers are in the following ranges:

Table 1: Flow characteristics around a superheater tube in typical PF power plants and mean values of measurements in Altbach (*calculated and **estimated values).

Description	Sym.	Unit	Min	Max	Altbach
Temp. FG	T_∞	°C	800	1200	1050
Temp. SH	T_W	°C	400	700	690
Tube diameter	D	mm	30	60	38
Velocity FG	u_∞	m/s	3	15	6.8*
O_2 content FG	x_{O2}	vol.-%	0	8	3.1
CO_2 content FG	x_{CO2}	vol.-%	10	18	15.3
H_2O content FG	x_{H2O}	vol.-%	2	20	6
Particle diam.	d_p	μm	0.02	200	21.4
Particle density	ρ_p	g/cm³	0.5	5.5	2.5**
Temp. gradient	∇T_g	K/mm	100	600	380

Min. and max. values:	Measurements in Altbach:
$400 < Re < 6{,}000$	$Re = 1{,}500$
$10 < Nu < 40$	$Nu = 19$
$Pr \approx Pr_W \approx 0.75$	$Pr = 0.75$
$10^{-6} < St < 50$	$St\ (d_{50}) = 0.46$
$0.003 < Kn < 5$	$Kn\ (T_\infty, d_{50}) = 0.034$
$4 < \Lambda < 80$	$\Lambda = k_p/k_g \approx 6\text{-}60$

Typical cylinder (tube) Reynolds numbers in a power plant are between Re = 400 and Re = 6,000, where the Reynolds number is defined as ($Re = \rho_g u_\infty D/\mu_g$), with the gas density ρ_g and dynamic viscosity μ_g. Gas properties are calculated depending on temperature and composition. In this Reynolds number range, the flow is in the subcritical regime with a laminar boundary layer and a three-dimensional turbulent wake (at the lee side of the cylinder). Transition in the shear layer is often observed in experiments.

The particle Stokes number (defined as the ratio of particle relaxation time and a typical flow time scale, $St = \rho_p d_p^2\ u_\infty/9\mu_g D$) shows a broad spectrum, with particles containing a high inertia (St = 50) and small, submicron particles perfectly following the streamlines ($St = 10^{-6}$). The diameter d_{50} (50% of the volume is below this diameter) yields a Stokes number of St = 0.46 for the deposition probe. At this Stokes number, the impaction probability (also called impaction efficiency η) of particles approaching the cylinder is around 70%. A particle with d_p = 10 μm has a lowered impaction probability of only 10%, indicating that inertial impaction is not responsible for small particles found in the deposit.

Two numbers are of particular importance for the thermophoretic force. First, the particle Knudsen number, which indicates whether the flow characteristics can be described by continuum mechanics (Kn < 1) or by methods of statistical mechanics. The Knudsen number is defined as the ratio of the mean free path length of gas molecules λ and the particle radius ($Kn = 2\lambda/d_p$). The mean free path length is a function of the gas temperature and calculated by $\lambda = 1.2533\mu_g(T_g R_s)^{1/2}/p$, where R_s is the specific gas constant, and p the gas phase pressure. Typical values in a power plant range from very low Kn numbers of 0.003 up to 5. This implies that small particles cannot be treated by continuum mechanics. The second number is the ratio of particle to gas thermal conductivity $\Lambda = k_p/k_g$. It is important to pay attention to the definition of this ratio, since it is sometimes defined inversely. The gas thermal conductivity is the translational part of the thermal conductivity calculated by $k_g = 15/4\mu_g R_s$ (Talbot et al. 1980). The particle thermal conductivity is also temperature-dependent and, more importantly, a strong function of the chemistry and physical state (molten or solid). Thermal conductivities of fly ash particles are reported within k_p = 0.3 - 4 W/(mK). Especially, iron-rich (Fe-rich) particles are assumed to have a considerably higher thermal conductivity than aluminosilicates (Al-Si) (Rezaei et al. 2000). Rezaei et al. 2000 gives values for the thermal conductivity of ashes dominated by aluminosilicates of around $k_{p,Al\text{-}Si}$ = 0.5 - 1.5 W/(mK) at a temperature of 1000°C. High temperature measurements of iron-rich slags or iron oxides are rare in the literature. Takeda et al. 2009 report values around $k_{p,Fe2O3}$ = 3 W/(mK) for Fe_2O_3 at 1000 °C.

THERMOPHORESIS AND NUMERICAL SIMULATION

A mathematical description of the thermophoretic force F_{th} in a non-dimensional form is given by:

$$\frac{F_{th}\rho_g}{\mu_g{}^2} = \Phi\frac{d_p\nabla T_g}{2T_g} \qquad (1)$$

In Eq. 1, ρ_p, μ_g, T_g are the density, dynamic viscosity and temperature which the gas would have at the centre of the particle position, if the particle is not present (Healy and Young 2010). ∇T_g is the temperature gradient in the gas phase, and Φ is a function of the Knudsen number and the thermal conductivity ratio $\Phi = \Phi(Kn, \Lambda)$. The temperature gradient strongly depends on the flow conditions. It is a function of the temperature difference between the flue gas and the superheater tube, and the free stream velocity which forms the boundary layer and its thickness. For the deposition probe in the Altbach power station, the maximum temperature gradient at the stagnation point (windward side) is approximately $\nabla T_g \approx 380$ K/mm. This value was obtained by CFD calculations shown in the results section.

The coefficient Φ has been described mathematically by different authors. Epstein 1929 first recognised the importance of the thermal conductivity ratio Λ and proposed an equation for Kn→0. Waldmann 1959 investigated the region of large Kn numbers, where values of Φ approach zero. Different correlations have been proposed for regions between 0.001 < Kn < 1. Most common is an expression by Talbot et al. 1980, who modified equations originally proposed by Brock 1962. Other correlations were introduced by Yamamoto and Ishihara 1988, Beresnev and Chernyak 1995, and, more recently, by Young 2011. The different expressions for Φ are summarised in a publication by Healy and Young 2010.

Fig. 3 shows different models for $-\Phi/2\pi$ as a function of the Knudsen number and different thermal conductivity ratios. The negative sign of this expression indicates the direction of thermophoresis towards the cold fluid or surface. It can be seen from Fig. 3, that with an increasing thermal conductivity ratio, the expression $-\Phi/2\pi$ decreases and thus the thermophoretic forces become smaller. Models by Yamamoto and Ishihara 1988 and Beresnev and Chernyak 1995 are impracticable since they use look-up tables and interpolation in between is required. In the region of small Knudsen numbers (0.003 < Kn < 1), models yield different values indicating high uncertainties. Young 2011 reviewed measurements in this region and found inconsistent data, which he explained by the difficulty of measuring such small forces. Even a negative thermophoretic force is predicted by the model of Young 2011 for very high particle thermal conductivities (Λ > 1000), which was first proposed in a theoretical work by Dwyer 1967. The grey-shaded area represents the region typical for a PF boiler, with particles in the size range of 0.2 < d_p < 200 μm and thermal conductivity ratios starting from around 4 up to 80. An examination of the two correlations of Talbot et al. 1980 and Young 2011 for an Al-Si and a Fe-rich particle is shown in Fig. 4. Calculations were carried out for conditions shown in Table 1 and for an average temperature gradient of ∇T_g = 230 K/mm. The thermophoretic force is expressed in the form of an acceleration by dividing it by the particle mass. Gravity is illustrated as a horizontal line. It can be seen that thermophoresis exceeds gravity for particles smaller than d_p = 20 μm depending on the model and particle chemistry. The

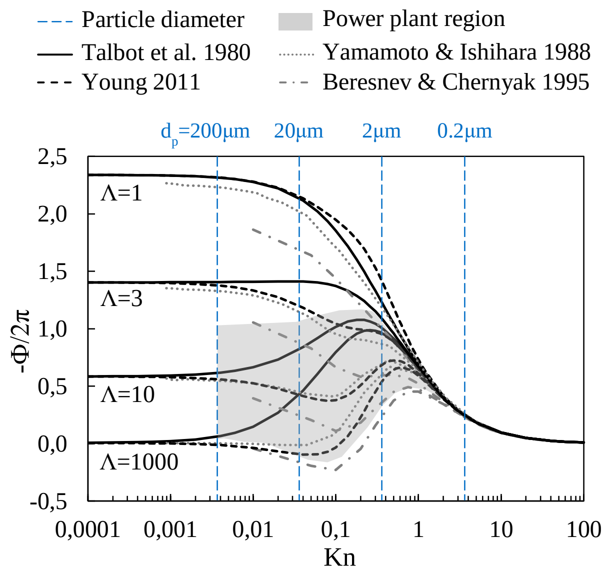

Fig. 3 Expression $-\Phi/2\pi$ as a function of Kn and Λ using different correlations. Typical particle diameters and Kn numbers found in power plants (calculated at T_g = 1000 °C) are shown.

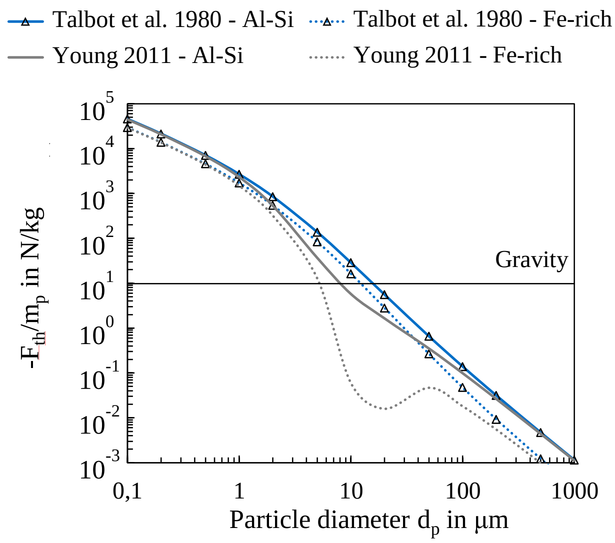

Fig. 4 Thermophoretic force as a function of particle diameter for an Al-Si (k_p = 1 W/mK) and Fe-rich (k_p = 3 W/mK) particle using the correlation of Talbot et al. 1980 and Young 2011.

model of Talbot et al. 1980 (lines with symbols in Fig. 4) predicts two similar curves for Fe-rich and Al-Si particles. Fe-rich particles experience a slightly lower thermophoretic force compared with Al-Si particles. The model of Young 2011 on the other hand, leads to a drastic decrease of the thermophoresic force in the region of particle diameters of 5 to 30 μm. If Young's expression of Φ is correct, the impaction probability of Fe-rich particles is very low, leading to deposits with only a small amount of Fe-rich particles in the size range of $5 < d_p < 30$ μm.

Numerical Simulation

The numerical model to study the impact of different thermophoretic models on deposition rates was set up in ANSYS FLUENT v16.0. A cylinder in the cross-flow is studied at three different Reynolds numbers. Fig. 5 shows the computational domain and its dimensions. The cylinder is set 5D in front of the domain centre Total dimensions are 30Dx20Dx1D, where D stands for the cylinder diameter. Inlet is defined as a velocity inlet with the freestream velocity u_∞ set to achieve the desired cylinder Reynolds number. An outflow boundary condition is chosen for the fluid leaving the domain. The top, bottom, front and rear walls are symmetry boundary conditions with no velocity gradient normal to the wall and a zero flux of all quantities across the boundary (slip wall condition). The Reynolds numbers studied in this paper are Re = 200, 1,500 and 3,900. For Re = 200, a two-dimensional grid with the same domain size as shown in Fig. 5 is used. Re = 200 was chosen since eddies in the wake do not show a three-dimensional structure and a laminar solver can be applied. This case serves for sensitivity studies on thermophoretic forces. The case with Re = 1,500 is based on measurements in the power plant. This case uses the conditions given in Table 1. Flue gas composition was used, species equations are solved, and gas properties are calculated in a mass-weighted and temperature-dependent way. Since, at Re = 1,500, the flow in the wake of the cylinder is three-dimensional and show turbulent structures,

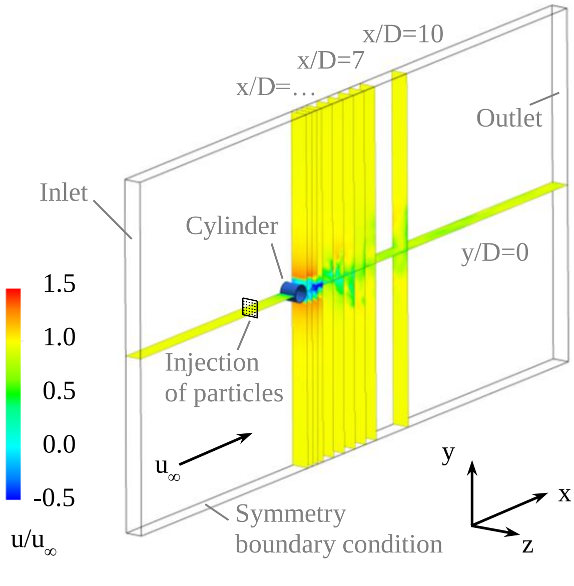

Fig. 5: Computational domain used for calculations.

turbulence is filtered in time and space using Large Eddy Simulations (LES). Sub-grid Scale (SGS) turbulence is modelled with the Smagorinsky-Lilly model, based on Boussinesq's approach. The dynamic Smagorinsky-Lilly model is chosen as suggested by Breuer 2000. The Re = 3,900 case is used for the validation of LES simulations. Validation is carried out against literature data on a cylinder in the cross-flow. Table 2 summarises all the test cases. Each case is either calculated with (ending -B), or without (-A) solving the energy equation. The isothermal cases (-A) are used to validate the flow field around the cylinder with literature data. Once the flow field is correct, the same settings are used including energy equation in order to solve the temperature field in the vicinity of the cylinder. Mass, momentum and energy equations are solved using second-order discretisation. The momentum equation for LES cases is solved using the bounded central differencing scheme. Pressure velocity coupling is achieved by using the SIMPLE algorithm (for this, see also ANSYS Fluent 2015).

The grid was generated in ANSYS ICEM CFD v16.0. The number of nodes in the x, y and z-direction is given in Table 2. The number of grid nodes for the LES cases is similar to Breuer 2000. The boundary layer of the cylinder is resolved by the placing of at least 10 nodes in the displacement thickness estimated by $\delta_1 = 0.335D/Re^{1/2}$, following the suggestion of Bouhairie and Chu 2007. The maximum y^+-value for the highest Reynolds number is y^+=0.6. The number of nodes around the circumference is set to at least 256 nodes for independent results (see Weber et al. 2013). The time step of transient simulations is chosen to ensure a Courant number smaller than unity for 95% of all cells. The maximum local Courant number did not exceed two.

Particles are injected at x = 3D further upstream of the cylinder as shown in Fig. 5. Particle trajectories are calculated using the Lagrangian formulation (Eq. 2):

$$\frac{d\vec{u}_p}{dt} = F_D(\vec{u}_g - \vec{u}_p) + \frac{\vec{g}(\rho_p - \rho_g)}{\rho_p} + \frac{\overrightarrow{F_{th}}}{m_p}, \qquad (2)$$

where $\vec{u}_p$, $\vec{u}_g$ are the particle and gas velocities, $\vec{g}$ the gravitational vector, and ρ_p, ρ_g the particle and gas densities at the current particle position. The term $F_D(\vec{u}_g - \vec{u}_p)$ is the drag force per unit mass, where F_D is calculated by:

$$F_D = \frac{18\mu_g}{\rho_p {d_p}^2}\frac{C_D Re_p}{24}. \qquad (3)$$

The drag coefficient C_D is dependent on the particle Reynolds number and calculated in a user-defined function (UDF). The equation is $C_D = a_1 + a_2/Re_p + a_3/Re_p$, where a_i are coefficients taken from Morsi and Alexander 1972. The particle Reynolds number is computed with $Re_p = (\rho_g d_p|\vec{u}_p - \vec{u}|)/\mu_g$. For very small particles and Kn > 1, the term F_D is calculated by Eq. 4 and Eq. 5:

$$F_D = \frac{1}{C_C}\frac{18\mu_g}{\rho_p {d_p}^2} \text{ with} \qquad (4)$$

$$C_C = 1 + Kn\left(1.257 + 0.4e^{-(1.1/Kn)}\right). \qquad (5)$$

Table 2: Investigated cases and their settings (grid size in number of nodes in x, y and z-direction, *Case 2-B uses settings from Table 1, right column, with the actual flue gas composition and gravity).

Case	T_∞ in °C	T_W in °C	Pr_∞	Pr_W	Fluid Prop.
Re=200 – 2D, laminar, transient, grid size 489x489x1					
Case-1-A	20	20	0.707	0.707	const.
Case-1-B1	1,000	800	0.707	0.707	const.
Case-1-B2	1,000	800	0.715	0.706	f(T)
Case-1-B3	1,000	600	0.715	0.694	f(T)
Case-1-B4	1,000	400	0.715	0.683	f(T)
Case-1-B5	1,000	200	0.715	0.682	f(T)
Re=1,500 – 3D, LES, transient, grid size 264x124x30*					
Case-2-B	1,050	690	0.753	0.752	f(T)
Re=3,900 – 3D, LES, transient, grid size 264x124x30					
Case-3-A	20	20	0.707	0.707	const.
Case-3-B	1,000	800	0.707	0.707	const.

The correction factor C_c is based on the work of Cunningham 1910 and adopted from Haugen and Kragset 2010. The acceleration, due to thermophoresis in Eq. 2, is included by means of a UDF according to Eq. 1.

RESULTS AND VALIDATION

This section is intended to summarize all the results obtained by the numerical simulation. Validation of the flow characteristics is carried out against the literature values of a circular cylinder in the cross-flow. A grid independence study investigating the impact of the number of nodes and the domain size had been carried out in a previous study (see Barnerßoi 2014). A domain size of 30x20D revealed independent results. Dimensionless experimental values are taken from various references. The drag coefficient C_D and the Strouhal number Str are taken from Schlichting and Gersten 2000. The pressure coefficient at the cylinder rear $-C_{bp}$ is taken from Willimason 1996. The separation point of the flow (measured from the front face stagnation point as shown in Fig. 7) Θ_s is taken from Bouhairie and Chu 2007, who summarised the literature values. The length of the recirculation zone L_F/D is taken from Norberg 1987. Heat transfer to the cylinder is validated by using the average Nusselt number, $\overline{Nu}$, around the cylinder circumference, the

Table 3: Comparison of averaged simulation results with experiments (shaded in grey). Literature values are taken from various references.

Case	C_D	Str	$-C_{pb}$	Θ_s
Re=200 Exp.	1.19-1.33	0.18-0.20	0.84-0.89	112
Case 1-A	1.37	0.200	0.954	111.9
Case 1-B1	1.37	0.203	0.947	111.6
Re=3,900 Exp.	0.98-0.99	0.215	0.90	85-86
Case 3-A	1.019	0.208	0.737	87.1
Case 3-B	0.989	0.232	0.765	87.2

Case	L_F/D	$\overline{Nu}$	Nu_s	Nu_r
Re=200 Exp.	0.99-1.11	6.6	13.8	5.2
Case 1-A	0.881	-	-	-
Case 1-B1	0.881	7.64	13.8	5.29
Re=3,900 Exp.	1.3-1.8	31-40	56-58	28-33
Case 3-A	1.486	-	-	-
Case 3-B	1.468	33.70	59.64	30.99

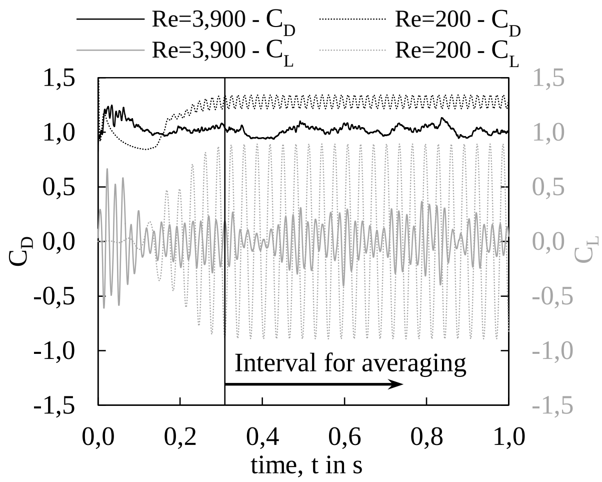

Fig. 6: Drag (black) and lift (grey) coefficient from simulation of Re = 200 (dotted line) and Re = 3,900 (continuous line); region used for averaging is illustrated.

local Nusselt number at the front face stagnation point, Nu_s, and the local Nusselt number at the cylinder rear, Nu_r. Experimental results for Re = 200 are taken from Eckert and Soehngen 1972, and, for Re = 3,900, from Sarma and Sukhatme 1977, and Krall 1969. Simulations are carried out as transient calculations and results are averaged for at least 20 shedding cycles. Fig. 6 shows the drag and lift coefficient as a function of time. Results are averaged once the fluctuations become stable, at around t = 0.3 s. The behaviour shown in Fig. 6 is similar to other numerical simulations (see Breuer 2000). Table 3 compares the simulation results with measurements for different cases. Both cases slightly over-predict the drag coefficient of the cylinder and the pressure coefficient in the wake of the cylinder. The Strouhal number, angle of separation of the flow, the recirculation length, and the Nusselt numbers agree well with the experimental values. Case 2-B is calculated using the measured flue gas composition, including gravity and temperature-dependent fluid properties. A comparison to experimental values is, therefore, not carried out, due to differing settings compared with measurements in the literature.

A comparison between the calculated and predicted Nusselt numbers around the circumference for cases 1 and 3 is illustrated in Fig. 7. Note that the literature data have slight deviations in the Reynolds number. In addition, the temperature difference between cylinder and fluid is typically small and differences in Pr can, therefore, be neglected. To account for this, the fluid properties were set to constant values in both cases. The laminar case 1 for Re = 200 agrees well with the measurements. For case 3, deviations at the stagnation point, and at the separation point of the flow, can be seen. Similar behaviour was found by Bouhairie and Chu 2007, who only showed instantaneous values. It can thus be summarized that the flow around a cylinder is predicted well with the commercial code, ANSYS Fluent. Deviations are mostly within measurement uncertainties and, therefore, the flow field can be used for calculating particle trajectories. When using LES simulations, it is essential to conduct a Stokes number analysis to determine the smallest particle, whose trajectory

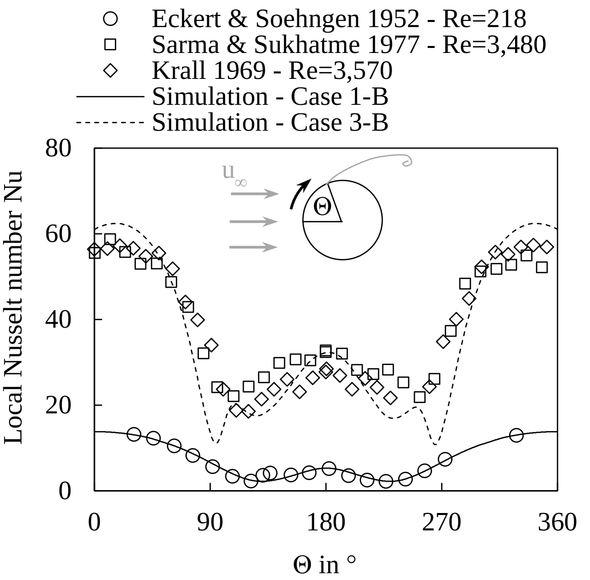

Fig. 7: Validation of the local Nusselt number around the circumference of the cylinder. (Note: literature data has slightly deviating Reynolds numbers).

can be predicted with the grid resolution. The procedure suggested by Pedel et al. 2014 was applied. Results indicate that sub-grid scale turbulence is of importance for particles smaller than d_p = 5 µm. Therefore, the majority of fly ash particles are unaffected by the SGS turbulence. In addition, in the vicinity of the cylinder, the grid resolution is high, resolving 98% of the turbulent scales.

The Re = 200 case was used to study the effect of thermophoresis on the particle impaction efficiency. A number of 10^6 particles are injected at x = 3D upstream of the cylinder, using the projected area of the cylinder as the inlet area. The impaction efficiency is defined as $\eta = n_{p,imp}/\ n_p$, where n_p stands for the number of injected particles and $n_{p,imp}$ is the number of particles impacted on the cylinder surface. The impaction efficiency is calculated using a UDF, which accounts for the interception mechanism. Particle trajectories are calculated for the particle centre and tracked as points, whereas in reality a particle might be in contact with the cylinder because of its size. This phenomenon is called interception (see also Haugen and Kragset 2010). A particle independence study revealed that calculating ten particle positions per cell and a number of 10^6 particles yield independent results.

Fig. 8 shows the impaction efficiency on the cylinder front face for all cases "1". Thermophoresis was considered by the expression of Talbot et al. 1980 using a thermal conductivity ratio of Λ = 10 (Al-Si particles). A set of temperature differences $\Delta T = T_\infty - T_W$ is used, and the impact on particle impaction efficiency is determined. Each point shown in Fig. 8 is a separate injection, which is defined by text files and set up using a Matlab script. If thermophoresis is neglected (ΔT = 0K), it can be seen that the impaction efficiency drops at a Stokes number of St = 0.3 ($d_p \approx 20$ µm) to very low values $\eta < 0.001$, indicating that only a small fraction of particles reaches the surface. The only particles impacting for small Stokes numbers are the ones injected at the cylinder centre (y=0). On the other hand, at large Stokes numbers St = 10, the impaction efficiency reaches values of up to 90%. Including the thermophoretic force, this leads to a strong increase in the impaction efficiency for small particles. At low Stokes numbers (St = 0.01), the probability of a particle impacting on the cylinder surface increases by almost four orders of magnitude, depending on the temperature differences and thus on the temperature gradient in the boundary layer. The higher the temperature difference, the more particles impact on the cylinder.

Fig. 9 shows the effect of the thermophoresis model and the thermal conductivity ratio. By including thermophoresis, the impaction efficiency again increases strongly for small particle diameters. However, the expression of Young 2011 leads to a decrease of around 80% for aluminosilicate particles (Λ = 10). For Fe-rich particles (Λ = 40), the

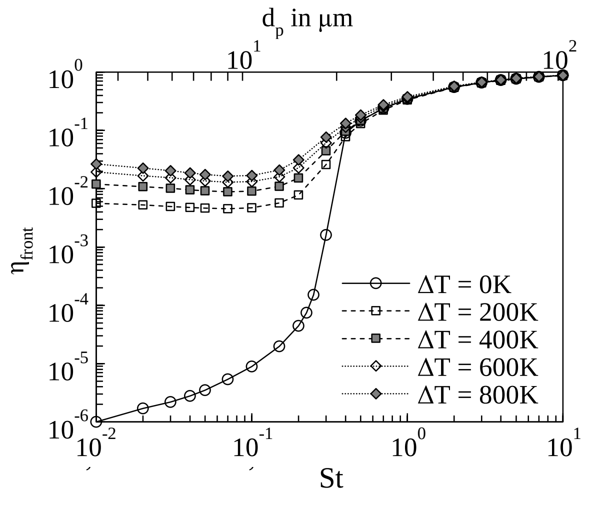

Fig. 8: Particle impaction efficiency as a function of the Stokes number and particle diameter for all Case 1 scenarios with Re = 200. Thermophoresis was accounted for with the model of Talbot et al. 1980 and Λ = 10.

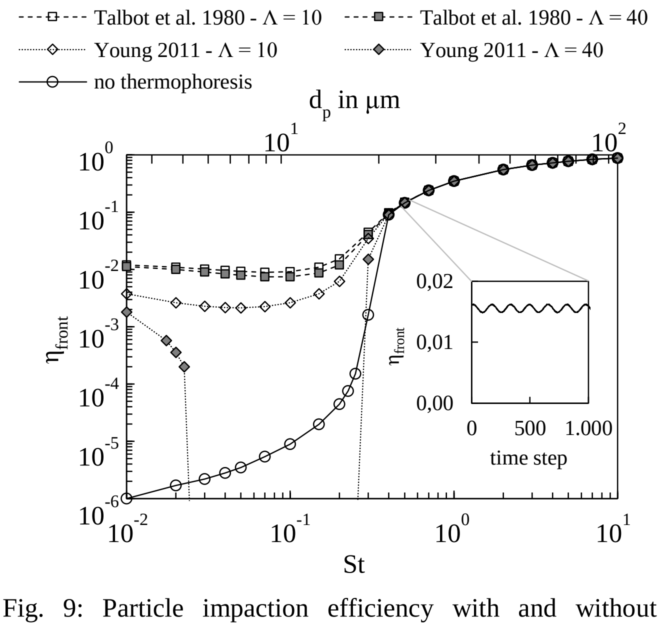

Fig. 9: Particle impaction efficiency with and without thermophoresis for case 1-B2. Comparison between the correlations of Talbot et al. 1980 and Young 2011 for two different thermal conductivity ratios (Al-Si: Λ = 10 and Fe-rich: Λ = 40).

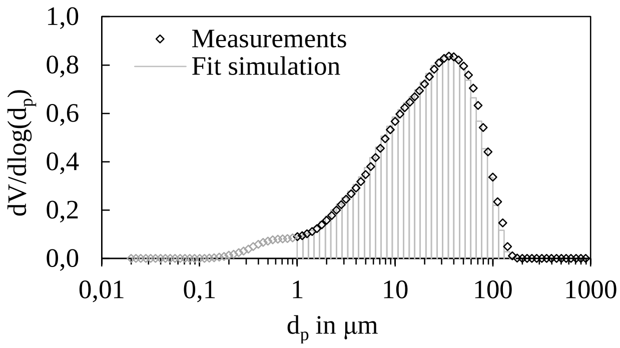

Fig. 10: Particle volume distribution measured in the Altbach power station upstream of the radiant superheater (location is shown in Fig. 1).

impaction efficiency drops at around St = 0.02 to zero, implying no particle impacts on the surface. This behaviour was expected based on the results shown in Fig. 2, and can explain why small iron-rich particles are only found in small quantities within the deposit. Based on these observations, the coefficient suggested by Young 2011 seems to be more adequate for the present case. However, the correlation has to be validated with further experiments. Fig. 9 also shows the time-dependence of the impaction efficiency for St = 0.4 and a clean tube (small window). It fluctuates with the same frequency as the drag coefficient. Thus, averaging is required and is carried out for three shedding cycles.

The Case 2-B is used to calculate impaction rates for the power plant measurements in Altbach with and without thermophoresis. The particle size distribution was measured by laser diffraction (Malvern Mastersizer 2000). Fly ash particles were sampled at the measurement location shown in Fig. 1. The measured volume distribution is given in Fig. 10. Particles were in the range of $0.1 < d_p < 175$ µm. In the simulation, the PSD was fitted using a Matlab code with a lower cut-off at $d_p = 1$ µm. Particles smaller than this cannot be calculated by Lagrangian tracking. In addition, SGS has an impact on the particle trajectory for such small diameters. Forty diameter classes are used and around $4x10^6$ are tracked in order to get independent results. The mass flow rate per particle is calculated using the power plant data and the measured PSD. A high number of small particles is necessary to ensure correct impaction efficiencies when only one out of a million particles impacts on the cylinder. Calculated impaction rates are given in Table 4. Although the difference in mass flow rate per unit area is marginal, the number of particles impacting due to thermophoresis is in the range of 10^7 additional particles per second and square metre, for a mean particle size of 10 µm particles.

DISCUSSION

It is shown that thermophoresis is an important mechanism for the early stages of ash deposition on a superheater tube. Measurements and numerical models

Table 4: Calculated impaction rates with and without thermophoresis (TP) for case 2-B (Altbach power station).

	Symbol	Unit	with TP	without P
Dep. rate	$\phi=\dot{m}/A$	kg/(m²s)	0.002669	0.002654

predict the impaction of a substantial number of fly ash particles due to thermophoresis, even for particles $d_p > 1$ µm. In addition, it is explained why particles with high thermal conductivity, such as iron-rich particles, show a significantly lower probability of impaction. This finding was confirmed qualitatively by EDX measurements. A number of 44 small particles were analysed in terms of composition and only five particles had an iron content higher than 10% with a maximum value of 40% (Babat et al. 2014). A quantitative evaluation is difficult, due to the presence of large iron-rich particles. A possible way could be the investigation of the cylinder rear, where no large iron-rich particles deposit. Particles could be scraped off and analysed. The results without TP are in line with findings by Haugen and Kragset 2010. Detailed CFD simulations considering thermophoresis for larger particles, and resolving the boundary layer, were not found in the literature and, therefore, present novel results. The statement of Walker et al. 1979 that thermophoresis plays an important role for diameters in the range of $0.1 < d_p < 10$ µm could be confirmed by using CFD methods.

The next step should cover the impact of surface roughness on deposition rates. The present study investigates an idealised clean tube which is only present at the early stages. In reality, deposit builts up, changes the flow field and leads to a pressure drop across the superheater and an increased thermal resistance. Therefore, a time-dependent model including the deposit built-up is desirable. In addition, a further study should investigate detailed sticking criteria in order to be able to predict the tendency of small particles to adhere to the cool surface. Radiation might also influence the particle temperature and should therefore be included. The reason for the small particle adherence might be due to the thermophoretic force still acting on settled particles, which migrated to the surface at low velocities. Furthermore, the sticking probability of low melting eutectics for iron-rich particles suggested by Babat et al. 2014 should be confirmed using CFD methods. With this approach, deposition rates could be calculated for the whole fly ash spectrum and could then finally be compared to measured deposition rates.

CONCLUSIONS

The main findings of this work are:

1. Thermophoresis is shown to play a dominant role during the early stages of deposit formation. LES simulations and Lagrangian tracking are used to estimate the impact of the thermophoretic force. It is shown that the impaction probability increases up to four orders of magnitude for a 5 µm particle within a temperature gradient of 380 K/mm in the boundary layer of a superheater tube.
2. Thermophoretic correlations presented in literature show huge differences in the region relevant for power plants. Recently suggested correlations seem to be more adequate. However, confirmation and more experimental validation is required.
3. The impaction of small aluminosilicate particles found in the power plant can be explained. Furthermore, the high thermal conductivity of iron-rich ash particles leads to a lowered deposition probability. Small iron-rich

particles (d_p < 20 μm) found in the fly ash experience a lower thermophoretic force and therefore, have a smaller impaction probability on the cylinder. This is in line with observations made in the power plant.

Further work should be devoted to the development of sophisticated particle-sticking criteria and their implementation into CFD codes, enabling the prediction of deposition rates.

ACKNOWLEDGMENTS

The authors would like to thank the support of “Energie Baden-Württemberg AG” (EnBW) for the cooperation in the frame of KW21. The research joint-venture is funded by the “Bayerisches Staatsministerium für Wissenschaft, Forschung und Kunst”, the “Ministerium für Wissenschaft, Forschung und Kunst Baden württemberg“ and EnBW. The work was carried out in the frame of the sub-project BY4DE.

NOMENCLATURE

A	area, m²
C	coefficient (e.g. drag or lift), dimensionless
d	diameter particle, m
D	diameter tube, m
F	force, N
k	thermal conductivity, W/(mK)
Kn	Knudsen number, dimensionless
n	number of particles, dimensionless
Nu	Nusselt number, dimensionless
p	pressure, Pa
Pr	Prantl number, dimensionless
R	specific gas constant, J/(kgK)
Re	Reynolds number, dimensionless
St	Stokes number, dimensionless
Str	Strouhal number, dimensionless
t	time, s
T	temperature, K
V	volume, m³
δ	boundary layer thickness, m
μ	dynamic viscosity, kg/(ms)
ρ	density, kg/m³
Θ	angle (circumferential position on cylinder), °
Φ	thermophoretic coefficient, dimensionless
Λ	thermal conductivity ratio, dimensionless
ϕ	deposition rate, kg/(m²s)

REFERENCES

ANSYS Fluent, 2015, Fluent Theory Guide 16.0

Babat, S., Spörl, R., Maier, J., and Scheffknecht, G., 2014, Investigation of Iron-rich Initial Layer Deposits at the Inlet of the Superheater Level in a Large Pulverized Fuel Power Plant, *Proceedings of the Impact of Fuel Quality Conference 2014*, Snowbird, USA, pp. 3-23, S

Barnerßoi, M., 2014, CFD-Modellierung der Partikelablagerungen durch Thermophorese an quer angeströmten Rohren, Diplomarbeit, *Techn. Uni. of Munich*

Baxter, L. L., 1993, Ash deposition during biomass and coal combustion: A mechanistic approach, *Biomass and Bioenergy*, Vol. 4 (2), pp. 85-102

Beresnev, S. and Chernyak, V., 1995, Thermophoresis of a Spherical Particle in a Rarefied Gas: Numerical Analysis based on the Model Kinetic Equations, *Physics of Fluids*, Vol. 7, Nr. 7, pp. 1743-1756

Bouhairie, S. and Chu, V. H., 2007, Two-dimensional simulation of unsteady heat transfer from a circular cylinder in crossflow, *J. of Fluid Mechanics*, Vol. 570, pp. 177-215

Breuer, M., 2000, A challenging test case for large eddy simulation: high Reynolds number circular cylinder flow, *Int. Journal of Heat and Fluid Flow*, Vol. 21, 648-654

Brock, J. R., 1962, On the theory of thermal forces acting on aerosol particles, *J. of Colloid S.*, Vol. 17, pp. 768-780

Cameron, J. H and Goerg-Wood, K., 1999, Role of Thermophoresis in the Deposition of Fume Particles Resulting from the Combustion of High Inorganic Containing Fuels with Reference to Kraft Black Liquor, *Fuel Processing Technology*, Vol. 60, pp. 49-68

Cunningham, E., 1910, On the Velocity of Steady Fall of Spherical Particles through Fluid Medium, *Proceedings of the Royal Society of London*, A83, No.563, pp. 357-365

Dwyer, H. A., 1967, Thirteen-Moment Theory of the Thermal Force on a Spherical Particle, *Physics of Fluids*, Vol. 10, pp. 976-984

Eckert, E. R. G. and Soehngen, E., 1972, Distribution of Heat-Transfer Coefficients Around Circular Cylinders in Crossflow at Reynolds Numbers From 20 to 500, *Journal of Basic Engineering*, Vol. 74, pp. 343-347

Epstein, P. S., 1929, Zur Theorie des Radiometers, *Zeitschrift für Physik*, Vol. 54, Nr. 7-8, pp. 537-563

Haugen, N. E. L. and Kragset, S., 2010, Particle Impaction on a Cylinder in a Crossflow as a Function of Stokes and Reynolds Numbers, *Journal of Fluid Mechanics*, Vol. 661, pp. 239-261

Healy, D. P. and Young, J. B., 2010, An Experimental and Theoretical Study of the Particle Deposition Due to Thermophoresis and Turbulence in an Annular Flow, *Int. Journal of Multiphase Flow*, Vol. 26, pp. 870-881

Kaer, S. K., Rosendahl, L. A. and Baxter, L. L., 2006, Towards a CFD-Based Mechanistic Deposit Formation Model for Straw-Fired Boilers, *Fuel*, Vol. 85, pp. 833-848

Krall, K. M., 1969, Local Heat Transfer around Transverse Circular Cylinder in Slip Flow, Ph.D. Thesis, *University of Minnesota*

Morsi, S. A. and Alexander, J. A., 1972, An Investigation of Particle Trajectories in Two-Phase Flow Systems, *Journal of Fluid Mechanics*, Vol. 55, pp.193-208

Norberg, C., 1987, Effects of Reynolds Number and a Low-Intensity Freestream Turbulence on the Flow Around a Circular Cylinder, Ph.D. Thesis, *Chalmers University*

Pedel J, Thornock, J. N., Smith, S. T. and Smith, P. J., 2014, Large Eddy Simulation of Polydisperse Particles in Turbulent Coaxial Jets Using the Direct Quadrature Method of Moments, *Int. J. of Multiphase Flow*, Vol. 63, pp. 23-38

Rezaei, H. R., Gupta, R. P., Bryant, G. W., Hart, J. T., Liu, G. S., Bailey, C. W., Wall, T. F., Miyamae, S., Makino, K. and Endo, Y, 2000, Thermal Conductivity of Coal Ash and Slags and Models Used, *Fuel*, Vol. 79, pp. 1697-1710

Sarma, T. S. and Sukhatme, S. P., 1977, Local Heat Transfer from a Horizontal Cylinder to Air in Cross Flow:

Influence of Free Convection and Free Stream Turbulence, *Int. Journal of Heat and Mass Transfer*, Vol. 20, pp. 51-56

Schlichting, H. and Gersten, K., 2000, Boundary-Layer Theory, *Springer Science & Business Media*

Takeda, M., Onishi, T., Nakakubo, S. and Fujimoto, S., 2009, Physical Properties of Iron-Oxide Scales on Si-Containing Steels at High Temperature, *Materials Transactions*, Vol. 50, No. 9, pp. 2242-2246

Talbot, L., Cheng, R. K., Schefer, R. W. and Willis, D. R. 1980, Thermophoresis of Particles in a Heated Boundary Layer, *Journal of Fluid Mechanics*, Vol. 101 (4), pp. 737-758

Waldmann, L., 1959, Über die Kraft eines inhomogenen Gases auf kleine suspendierte Kugeln, *Zeitschrift für Naturforschung*, Vol. 14a, Nr. 7, pp. 589-599

Walker, K. L., Homsy, G. M. and Geyling, F. T., 1979, Thermophoretic Deposition of Small Particles in Laminar Tube Flow, *J. of Colloid and Interf. Sc.*, Vol. 69, pp. 138-147

Weber, R., Schaffel-Mancini, N., Mancini, M. and Kupka, T., 2013, Fly Ash Deposition Modelling: Requirements for Accurate Predictions of Particle Impaction on Tubes, *Fuel*, Vol. 108, pp. 586-596

Williamson, C. H. K., 1996, Vortex Dynamics in the Cylinder Wake, *Annual Review of Fluid Mechanics*, Vol. 28, pp. 477-539

Yamamoto, K. and Ishihara, Y., 1988, Thermophoresis of a Spherical Particle in a Rarefied Gas of a Transition Regime, *Physics of Fluids*, Vol. 31, pp. 3618-3624

Young, B. J., 2011, Thermophoresis of a Spherical Particle: Reassessment Clarification, and New Analysis, *Aerosol Science and Technology*, Vol. 45, pp. 927-94